Flow Turbulence Combust (2010) 84:193–218
DOI 10.1007/s10494-009-9220-4

Towards a Unified Turbulence Simulation Approach for Wall-Bounded Flows

Kun-Jung Hsieh · Fue-Sang Lien · Eugene Yee

Received: 10 April 2008 / Accepted: 4 May 2009 / Published online: 16 May 2009

Abstract A hybrid Reynolds-averaged Navier–Stokes/Large-Eddy Simulation (RANS/LES) methodology has received considerable attention in recent years, especially in its application to wall-bounded flows at high-Reynolds numbers. In the conventional zonal hybrid approach, eddy-viscosity-type RANS and subgrid scale models are applied in the RANS and LES zones, respectively. In contrast, the non-zonal hybrid approach uses only a generalized turbulence model, which provides a unified simulation approach that spans the continuous spectrum of modeling/simulation schemes from RANS to LES. A particular realization of the non-zonal approach, known as partially resolved numerical simulation (PRNS), uses a generalized turbulence model obtained from a rescaling of a conventional RANS model through the introduction of a resolution control function F_R, where F_R is used to characterize the degree of modeling required to represent the unresolved scales of turbulent motion. A new generalized functional form for F_R in PRNS is proposed in this study, and its performance is compared with unsteady RANS (URANS) and LES computations for attached and separated wall-bounded turbulent flows. It is demonstrated that PRNS behaves similarly to LES, but outperforms URANS in general.

Keywords Turbulence modeling · RANS · LES · Hybrid RANS/LES · Wall-bounded turbulent flows

K.-J. Hsieh · F.-S. Lien (✉)
Department of Mechanical and Mechatronics Engineering, University of Waterloo, Waterloo, Ontario, N2L 3G1, Canada
e-mail: fslien@uwaterloo.ca

E. Yee
Defence R&D Canada—Suffield, P.O. Box 4000, Medicine Hat, Alberta, T1A 8K6, Canada

1 Introduction

The Reynolds-averaged Navier–Stokes (RANS) approach has been widely used to simulate turbulent flows encountered in many industrial and engineering applications. In the RANS approach where only the time- (or ensemble-)averaged flow properties are resolved and all other scales of motion are modeled, the computational cost of turbulent flows at high-Reynolds numbers is relatively low. However, the RANS approach can perform poorly in calculating complex flows (such as bluff body flows) which are dominated by coherent large-eddy structures. Because the turbulence models used in RANS are empirically tuned to optimize their performance in simple and thin shear flows where the mean pressure gradient and mean streamline curvature are small, RANS is unable to capture correctly the geometry-dependent large eddies in many complex flows (e.g., three-dimensional flows).

On the other hand, these large eddies can be accurately predicted using large-eddy simulation (LES) because the unsteady large-scale turbulent motions are explicitly resolved in LES. Unfortunately, the application of LES to wall-bounded flows at high-Reynolds numbers is severely restricted, owing to the requirement for a fine-grid resolution to resolve the small-scale flow motions near the wall. One strategy to reduce the high computational cost incurred here is to model (rather than resolve) the turbulence in the near-wall region. The simplest method to accomplish this is to use a wall stress model (analogous to a wall function in the RANS approach) to mimic the effects of the near-wall turbulence. In this approach, an algebraic relationship between the wall shear stress and the velocity at the first off-wall grid node is assumed. Schumann [36] proposed the first wall stress model based on an equilibrium law-of-the-wall relationship, and his model was further improved by Grotzbach [14] and Piomelli et al. [31]. However, the validity of the application of these wall stress models to separated flows is questionable, because the simple law-of-the-wall relationship does not account for the effects of the (either favorable or adverse) pressure gradient.

To reduce the significant computational cost of LES, while improving on the predictive accuracy of RANS over a broad range of turbulent flows, the application of a hybrid RANS/LES methodology has been proposed. The concept underlying this methodology is to combine the computational efficiency of RANS for modeling the flow in the near-wall regions, with the predictive accuracy of LES for simulating the large-scale turbulent flow structures in regions away from the walls (or, any other solid surfaces). In general, hybrid methods can be classified into two major categories: namely, zonal and non-zonal approaches. In the zonal approach, the computational domain is divided into distinct RANS and LES zones, in which conventional RANS and subgrid scale (SGS) turbulence models (e.g., k–ε turbulence closure and Smagorinsky model) are used in the RANS and LES zones, respectively. The RANS and LES solutions are coupled through the interface between these two zones, where information on the flow is exchanged (two-way interaction). The interface location that separates the two zones can be explicitly specified by a given wall-normal distance (e.g., [8, 45]) or dynamically determined based on the RANS and LES turbulence length scales [46].

Owing to the different averaging procedures used in the RANS (statistical averaging) and LES (spatial filtering) regions, which give considerably different spectral properties in the RANS and LES solutions, there is an incompatibility of the flow

properties around the modeling interface in the zonal approach. A good example of the effect of this incompatibility on the prediction of the flow can be found in the simulation of a plane channel flow, where a non-physical *buffer-like* layer (see, e.g., [19]) appears in the vicinity of the modeling interface between the RANS and LES regions. This incompatibility between RANS and LES can result in unphysical discontinuities in the flow quantities (e.g., velocities or eddy viscosities) across the interface. Several strategies have been proposed to circumvent this problem. Temmerman et al. [45] damped the modeled RANS turbulence in the vicinity of interface to reduce the total turbulence in the RANS zone. Another remedy is to introduce forcing to increase the resolved turbulence around the interface. The forcing can be obtained either from a stochastic backscatter model [32], or from turbulent fluctuations either synthesized [6] or extracted from a reference direct numerical simulation (DNS) or LES database [7, 18].

In the non-zonal approach, a single generalized turbulence model is used in the entire computational domain. This approach offers a unified simulation framework that spans the continuous spectrum of flow simulation/modeling schemes from RANS to LES (and even DNS). In these schemes, the generalized turbulence model can function as a RANS turbulence closure model or as a LES SGS stress model, depending on the local grid resolution or flow properties. From a theoretical point of view, the unified modeling approach can be achieved in principle by applying a temporal filter to the Navier–Stokes equations in the manner suggested by Liu and Shih [24]. The "width" of this temporal filter defines explicitly which scales of the turbulent flow motion are resolved. Depending on the width of the temporal filter (or, equivalently, cutoff frequency) imposed on the Navier–Stokes equations, the velocities obtained from the simulation can be interpreted as a statistical average as in RANS, as partially resolved large-scale velocity fluctuations as in LES, or as fully resolved (instantaneous) velocity fluctuations as in DNS. Since there is no zonal interface in this approach, the flow properties across the entire computational domain are continuous everywhere.

A well-known example of the non-zonal approach is the detached-eddy simulation (DES) introduced by Spalart et al. [41]. In the original DES formulation, the one-equation Spalart–Allmaras (SA) model [40] for the turbulent viscosity was used. Here, the SA model (which was designed originally for aerodynamic flows) is utilized in such a way that it behaves as a SGS model when the model length scale switches from the use of a wall-normal distance (RANS length scale) to a grid spacing (LES length scale). In general, DES can be formulated with any RANS model, simply by modifying the turbulence length scale used in the RANS model. For example, Strelets [44] modified the length scale used in the modeling of the viscous dissipation term of the k-equation to give a DES based on the k–ω turbulence model (where k and ω denote the turbulent kinetic energy and the frequency characteristic of the integral time scale for turbulence, respectively). Successful applications of DES to various massively separated flows were reported by Strelets [44] and Squires et al. [43]. However, when Nikitin et al. [29] and Piomelli et al. [32] used DES to simulate plane channel flow, they found that DES produced a non-physical buffer layer, similar to that observed in the zonal approach.

In another type of non-zonal approach, a generalized turbulence model is obtained by rescaling a conventional RANS model through the introduction of a resolution control function F_R. Since RANS and LES have the same form of filtered

transport equations, the unknown turbulent stress tensor τ_{ij} in the filtered momentum equation can be modeled as $\tau_{ij} = F_R \tau_{ij}^{RANS}$, where τ_{ij}^{RANS} is the modeled Reynolds stress tensor available from a RANS model. The role of F_R is to characterize the degree of modeling required to represent the unresolved scales of turbulent flow motion. A constraint on F_R is that its value must be confined to lie in the range between zero and one. The generalized turbulence model behaves as a RANS model when $F_R \to 1$, in the sense that all scales of the turbulent flow motion are modeled in this case. Alternatively, when $F_R \to 0$, the generalized turbulence model vanishes and the simulation behaves as DNS in the sense that all scales of the turbulent flow motion are resolved explicitly. In between these two limits, the generalized turbulence model behaves as a LES-type subscale stress model in the sense that only the scales of turbulent flow motion smaller than the filter width are modeled. This approach was first introduced by Speziale [42], and has been modified and generalized in the form of the flow simulation methodology (FSM) advocated by Fasel et al. [10], the limited numerical scales (LNS) approach proposed by Batten et al. [1], the partially averaged Navier–Stokes (PANS) method developed by Girimaji [13], and the partially resolved numerical simulation (PRNS) scheme introduced by Liu and Shih [24]. In this paper, we will use the acronym PRNS to refer generically to all these similar strategies.

The objective of this study is to propose a generalized functional form for F_R. The performance of this proposed functional form in PRNS, in comparison with the unsteady RANS (URANS) and LES calculations, will be evaluated against two wall-bounded turbulent flows that are fully developed, namely, a plane channel flow (attached flow) and a flow over a wall-mounted matrix of cubes in a plane channel (separated flow). These fully-developed turbulent flows are useful for the validation of the numerical modeling and simulation, because streamwise and spanwise periodic conditions can be applied in the numerical computation, eliminating the need to specify appropriate inflow, outflow and lateral boundary conditions for the problem.

2 Mathematical Formulation

2.1 Governing equations

Applying a filter (or averaging operator) to the governing equations for the conservation of mass and momentum for an incompressible fluid flow yields

$$\frac{\partial \overline{u}_j}{\partial x_j} = 0, \tag{1}$$

$$\frac{\partial \overline{u}_i}{\partial t} + \frac{\partial}{\partial x_j}\overline{u}_j\overline{u}_i = -\frac{1}{\rho}\frac{\partial \overline{p}}{\partial x_i} + \frac{\partial}{\partial x_j}\left(2\nu\overline{S}_{ij} - \tau_{ij}\right), \tag{2}$$

where $\overline{S}_{ij} = \left(\partial\overline{u}_i/\partial x_j + \partial\overline{u}_j/\partial x_i\right)/2$ is the filtered strain-rate tensor, and τ_{ij} is the turbulent stress tensor which arises as a result of the filtering procedure. Depending on the applied filter, an overbar will be used to denote an ensemble-averaged, a spatially-filtered, or a temporally-filtered flow quantity in URANS, LES, and PRNS,

respectively. Note that in the case of an inhomogeneous filter, the commutation errors in (1) and (2) are assumed to be negligible here.

2.2 URANS

For unsteady flows in the RANS approach, an ensemble-averaged variable is defined as

$$\overline{\phi}(x_i, t) = \lim_{N\to\infty} \frac{1}{N} \sum_{n=1}^{N} \phi_n(x_i, t), \tag{3}$$

where N is the number of flow realizations. The Reynolds stresses, required for the closure of the ensemble-averaged momentum equation, is commonly modeled using the Boussinesq eddy-viscosity approximation, which assumes a linear relationship between the turbulent stress and mean strain-rate tensors:

$$\tau_{ij}^{RANS} \equiv \overline{u_i' u_j'} = \frac{2}{3} k \delta_{ij} - 2\nu_t \overline{S}_{ij}, \tag{4}$$

where u_i' is the fluctuating velocity in the x_i-direction, ν_t is the eddy viscosity and $k \equiv \overline{u_i' u_i'}/2$ is the (total) turbulent kinetic energy. Within the framework of the standard (high-Re number) k–ε model (where ε is the dissipation rate of k), the eddy viscosity is determined as

$$\nu_t = C_\mu \frac{k^2}{\varepsilon}. \tag{5}$$

The modeled transport equations for k and ε in the standard k–ε model are given by

$$\frac{\partial k}{\partial t} + \frac{\partial}{\partial x_j} \overline{u}_j k = \frac{\partial}{\partial x_j} \left(\frac{\nu_t}{\sigma_k} \frac{\partial k}{\partial x_j} \right) + P_k - \varepsilon, \tag{6}$$

$$\frac{\partial \varepsilon}{\partial t} + \frac{\partial}{\partial x_j} \overline{u}_j \varepsilon = \frac{\partial}{\partial x_j} \left(\frac{\nu_t}{\sigma_\varepsilon} \frac{\partial \varepsilon}{\partial x_j} \right) + \frac{\varepsilon}{k} \left(C_{\varepsilon 1} P_k - C_{\varepsilon 2} \varepsilon \right), \tag{7}$$

where $P_k \equiv -\tau_{ij}^{RANS} \partial \overline{u}_i / \partial x_j = 2\nu_t \overline{S}_{ij} \overline{S}_{ij}$ is the (modeled) production of turbulent kinetic energy. The closure coefficients in the standard k–ε model are given by [20]

$$C_\mu = 0.09,\ \sigma_k = 1.0,\ \sigma_\varepsilon = 1.3,\ C_{\varepsilon 1} = 1.44,\ \textit{and}\ C_{\varepsilon 2} = 1.92. \tag{8}$$

These closure coefficients have been determined by a comprehensive data fitting over a wide range of canonical flows which include some thin turbulent shear flows.

2.3 LES

In LES, the large scales of motion in the turbulent flow are directly computed, whereas the effects of the small scales of motion in the flow (which cannot be explicitly resolved) are modeled. The equation of motion for the filtered velocity field computed in LES can be obtained by applying a low-pass spatial filter to the Navier–Stokes equations, which results in the separation of the large and small scales

of turbulent motion in the flow. If a top-hat spatial filter with width $\overline{\Delta}$ is used, a spatially-filtered large-scale flow variable is given by

$$\overline{\phi}(x_i, t) = \frac{1}{\overline{\Delta}} \int_{x_i - \overline{\Delta}/2}^{x_i + \overline{\Delta}/2} \phi(x_i', t)\, dx_i'. \tag{9}$$

In most practical applications of LES performed using a finite-volume discretization method, an implicit filter (i.e., volume averaging) is applied in which the inhomogeneous spatial filter width $\overline{\Delta}$ is related to the grid spacing used in the discretization of the computational flow domain.

The most popular SGS stress model is undoubtedly the Smagorinsky model [39], which is a zero-equation eddy viscosity model based on a simple mixing length approach. In this model, the SGS stresses are represented as

$$\tau_{ij}^{SGS} \equiv \overline{u_i u_j} - \overline{u}_i \overline{u}_j = \frac{1}{3}\tau_{kk}^{SGS}\delta_{ij} - 2\nu_t^{SGS}\overline{S}_{ij}, \tag{10}$$

where the SGS viscosity is given by

$$\nu_t^{SGS} = (C_s\overline{\Delta})^2 \sqrt{2\overline{S}_{ij}\overline{S}_{ij}}. \tag{11}$$

The model constant C_s usually assumes a value between 0.1 and 0.2, depending on the particular flow. For example, Lilly [23] obtained $C_s \approx 0.17$ for homogeneous isotropic turbulence, whereas Deardorff [9] suggested that $C_s = 0.1$ for a plane channel flow. One weakness of the Smagorinsky model is that ad-hoc adjustments of C_s are required in different types of turbulent flow. To overcome this problem, Germano et al. [12] proposed a dynamic procedure which dynamically computes C_s at every grid point in space and at every time step. However, the dynamic procedure may result in negative values for C_s, and this can lead to numerical instability or even divergence in the flow simulation. In this paper, $C_s = 0.1$ will be used in our simulations of wall-bounded flows.

2.4 PRNS

Liu and Shih [24] defined a temporally-filtered large-scale flow variable in PRNS using a homogeneous top-hat temporal filter with width Δ_T, so

$$\overline{\phi}(x_i, t) = \frac{1}{\Delta_T} \int_{t - \Delta_T/2}^{t + \Delta_T/2} \phi(x_i, t')\, dt'. \tag{12}$$

It can be seen that $\overline{\phi}$ becomes a Reynolds-averaged (or, equivalently time-averaged) flow quantity as $\Delta_T \to \infty$, and $\overline{\phi}$ becomes an instantaneous flow quantity as $\Delta_T \to 0$. It should be noted that the temporal and spatial filtering operations used in PRNS and LES are intimately linked (see, e.g., [34]). Let $\overline{\Delta}_c$ be the cutoff length of a spatial filter. The corresponding cutoff wave number for this spatial filter is $\kappa_c = 2\pi/\overline{\Delta}_c$. Let $E(\kappa)$ denote the spectral energy density of the velocity fluctuations. The kinetic energy of the velocity fluctuations associated with eddies of size $\overline{\Delta}_c = 2\pi/\kappa_c$ (cutoff length scale) is $\kappa_c E(\kappa_c)$, and this cutoff length scale is associated with a cutoff velocity scale given by $v_c = \sqrt{\kappa_c E(\kappa_c)}$. In view of this, the cutoff time scale t_c for a temporal

filter must be related to the cutoff length scale $\overline{\Delta}_c$ for the equivalent spatial filter as $t_c = \overline{\Delta}_c / v_c$. When an implicit filter is used in PRNS, Δ_T is related to the time step Δt used in the simulation and this time step must be appropriately selected so as to be consistent with the grid spacing $\overline{\Delta}$.

The subscale stress tensor in the framework of PRNS is modeled as

$$\tau_{ij}^{PRNS} \equiv \overline{u_i u_j} - \overline{u}_i \overline{u}_j = F_R \tau_{ij}^{RANS}, \tag{13}$$

where F_R is a resolution control function whose value lies between zero and one. Depending on the physical resolution requirements, PRNS can behave as URANS when $F_R \to 1$ or as DNS when $F_R \to 0$. Between these two limits, PRNS behaves as some form of LES (either very large eddy simulation (VLES) when using relatively coarse grids through to near-wall resolved LES when using very fine grids). The predictive accuracy of PRNS depends on the value of F_R, as well as on the specific formulation of the turbulence model. In order to give a proper representation of τ_{ij}^{PRNS} in a complex turbulent flow, a two-equation eddy-viscosity-based turbulence model (e.g., the k–ε model) is often needed. Accordingly, (13) has the explicit form

$$\tau_{ij}^{PRNS} = F_R \left(\frac{2}{3} k \delta_{ij} - 2 \nu_t \overline{S}_{ij} \right) = \frac{2}{3} F_R k \delta_{ij} - 2 \nu_t^{PRNS} \overline{S}_{ij}, \tag{14}$$

where $\nu_t^{PRNS} = F_R \nu_t$ is the subscale eddy viscosity for PRNS. In practice, the term $\frac{2}{3} F_R k \delta_{ij}$ in (14) is absorbed into the filtered pressure term in (2) when solving the transport equation for the filtered momentum.

Several formulations for F_R have been introduced in the literature, and most of these involve a function that depends on the ratio of a physical turbulence length scale to a computational grid size ($\overline{\Delta}$). Speziale [42] proposed

$$F_R = \left[1 - \exp\left(-\beta \overline{\Delta} / l_K \right) \right]^n, \tag{15}$$

where l_K is the Kolmogorov length scale (whose value can be determined from a RANS model), and β and n are closure constants. In (15), $\overline{\Delta}/l_K$ is a measure of local resolution of the computational grid. When the grid resolution is very coarse relative to the smallest physical scales of turbulent flow motion as embodied by the Kolmogorov length scale (i.e., $\overline{\Delta}/l_K \to \infty$), $F_R \to 1$. Similarly, when the grid resolution is fine enough to resolve all the physical scales of motion in the turbulent flow (i.e., $\overline{\Delta}/l_K \to 0$), $F_R \to 0$.

Alternatively, Shih and Liu [37] suggested

$$F_R \geq \left(\frac{\overline{\Delta}}{l_{RANS}} \right)^{4/3} \left(\frac{k}{k_{RANS}} \right)^{-2}, \tag{16}$$

where l_{RANS} and k_{RANS} are the characteristic turbulence length scale and turbulent kinetic energy determined from a RANS model, respectively, and k is the unresolved (or subscale) turbulent kinetic energy in PRNS. This result for F_R generalizes the formulation given by Liu and Shih [24]. It is important to note that (16) only provides an estimate for the smallest value of F_R that a given computational grid can support. A constraint for F_R that is similar to (16) has also been proposed by Lakshmipathy and Girimaji [17]. However, rather than using the integral length scale l_{RANS} for turbulence in the constraint for F_R, Lakshmipathy and Girimaji argued alternatively for the use of the Taylor microscale as the characteristic length scale. More recently,

Shih and Liu [38] proposed an alternative formulation for F_R, which advocates the utilization of a user pre-specified (constant) value for F_R (between zero and one) with the interpretation that F_R corresponds to the fraction of the total turbulent kinetic that is not resolved in the simulation. Given any user-specified value for F_R, Shih and Liu further suggest that a grid-independent solution can be obtained by using a sufficiently refined grid (viz., for a sufficiently small grid size so as to resolve all the relevant turbulence scales that contribute to the fraction of the total turbulent kinetic energy that is permitted by the chosen value for F_R).

A generalized functional form for F_R based on the turbulence energy spectrum is proposed in the present study. When the cutoff wave number κ_c lies within the inertial sub-range scales of motion for the turbulence (see Fig. 1), the energy spectrum $E(\kappa) \propto \varepsilon^{2/3}\kappa^{-5/3}$ $(\kappa_i \le \kappa_c \le \kappa_K)$ where κ_i and κ_K are the wave numbers corresponding to the integral and Kolmogorov scales of turbulence, respectively. In view of this, our proposed functional form for $F_R \equiv F_R(\kappa_i, \kappa_c, \kappa_K)$ is given by

$$F_R = \frac{\int_{\kappa_c}^{\kappa_K} E(\kappa)\, d\kappa}{\int_{\kappa_i}^{\kappa_K} E(\kappa)\, d\kappa} = \frac{\kappa_K^{-2/3} - \kappa_c^{-2/3}}{\kappa_K^{-2/3} - \kappa_i^{-2/3}}, \tag{17}$$

where the definite integrals in the numerator and denominator of (17) represent the areas under the energy spectrum curve between κ_c and κ_K and between κ_i and κ_K, respectively. Therefore, F_R in (17) roughly resembles the ratio of the unresolved turbulence kinetic energy [approximated by $\int_{\kappa_c}^{\kappa_K} E(\kappa)\, d\kappa$] to the total turbulence kinetic energy [approximated by $\int_{\kappa_i}^{\kappa_K} E(\kappa)\, d\kappa$]. Note that in a practical implementation, κ_c is replaced by $\max[\kappa_i, \min(\kappa_c, \kappa_K)]$ in order to ensure the condition $F_R = 0$ when $\kappa_c \ge \kappa_K$, and $F_R = 1$ when $\kappa_c \le \kappa_i$. The wave number is related to the length scale as

$$(\kappa_i, \kappa_c, \kappa_K) = 2\pi\left(l_i^{-1}, l_c^{-1}, l_K^{-1}\right), \tag{18}$$

where $l_i = C_\kappa k^{3/2}/\varepsilon$, l_c, and $l_K = \left(\nu^3/\varepsilon\right)^{1/4}$ are the integral, filter cutoff and Kolmogorov length scales, respectively. The quantities k and ε used here are obtained from the same turbulence model [e.g., (6) and (7)] as used in RANS, except that it is the time-dependent resolved velocities (i.e., $\overline{u}_i$ obtained from the filtered momentum equation) rather than the ensemble-averaged velocities that are coupled to the transport equations for k and ε. The time-dependent resolved velocities enter the

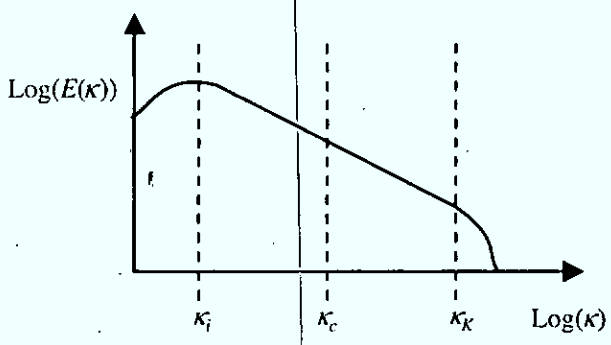

Fig. 1 Schematic view of the energy spectrum of the turbulent velocity

transport equations for k and ε in two ways: (1) through the advection term and (2) through the turbulence energy production term $P_k \left(= 2\nu_t \overline{S}_{ij}\overline{S}_{ij}\right)$.

If we consider the decomposition $\overline{u}_i = \langle \overline{u}_i \rangle + u_i''$, where $\langle \overline{u}_i \rangle$ is the time-averaged (or ensemble-averaged) value of $\overline{u}_i$, and u_i'' is the departure of $\overline{u}_i$ from $\langle \overline{u}_i \rangle$, it can be shown that $P_k = 2\nu_t \overline{S}_{ij}\overline{S}_{ij}$, computed using $\overline{u}_i$ (as in PRNS), is larger than that computed using $\langle \overline{u}_i \rangle$ (as in RANS). In consequence, PRNS will predict larger values for k and ε (since P_k appears in both the k and ε equations) than RANS. Although the k and ε predicted by the PRNS approach are different from those obtained with the RANS approach, it is expected that the resulting integral length scale, $l_i \propto k^{3/2}/\varepsilon$, has approximately the same order of the magnitude, and the differences in this length scale as determined using the turbulence quantities k and ε in either PRNS or RANS can be compensated through the introduction of the closure constant C_κ in the definition of l_i. Alternatively, k and ε can be obtained from a separate RANS calculation, but this option is computationally more expensive.

Speziale [42] noted that the estimation of l_K to an accuracy of 10% only requires that ε be estimated to an accuracy of 50%. As a consequence, a reasonably accurate value of l_K can be obtained from a prediction of ε using standard turbulence closure models. The only parameter in the formulation of F_R, which requires calibration, is the closure constant C_κ in l_i. When the value of C_κ (and consequently l_i) increases, the value of κ_i [defined in (18)] decreases. As a result, the value of F_R decreases because the value of the definite integral in the denominator of (17) increases (owing to the smaller value of κ_i). The optimal value of C_κ will need to be determined over a range of flow conditions. For the standard k–ε turbulence model used with PRNS, $C_\kappa = 40$ was used for this study. This value was chosen based on a preliminary calibration using the test problems described herein.

For the characteristic length scale associated with the cutoff wave number, we set

$$l_c = 2\max\left(\overline{\Delta}, \left|\overrightarrow{u}\right| \Delta t\right), \tag{19}$$

where $\overline{\Delta} = \left(\Delta_x \Delta_y \Delta_z\right)^{1/3}$ is the local grid size, and $\overrightarrow{u}$ is the local convection velocity in the cell. The additional factor of 2 accounts for the Nyquist frequency imposed by the finite size of a grid cell (i.e., a grid cell of size $\overline{\Delta}$ cannot resolve a flow structure smaller than $2\overline{\Delta}$). The time step Δt is also included because the time step should be small enough to resolve adequately the advective transport of any grid-resolved flow structure. The size of time step is estimated using the Courant–Friedrichs–Lewy (CFL) condition:

$$CFL = \frac{\left|\overrightarrow{u}\right| \Delta t}{\overline{\Delta}} \leq 1. \tag{20}$$

Owing to the imposed CFL condition in which $\left|\overrightarrow{u}\right| \Delta t \leq \overline{\Delta}$, the cutoff length scale in (19) becomes $l_c = 2\overline{\Delta}$. In summary, the length scales required to calculate wave numbers in (18) are as follows:

$$\left(l_i, l_c, l_\kappa\right) = \left[C_\kappa k^{3/2}/\varepsilon, 2\left(\Delta_x \Delta_y \Delta_z\right)^{1/3}, \left(\nu^3/\varepsilon\right)^{1/4}\right]. \tag{21}$$

Our proposed PRNS approach differs from most of the other PRNS approaches (e.g., FSM or LNS) which generally utilize a "reduced" eddy viscosity [e.g., ν_t^{PRNS} in (14)]

in the momentum equation, as well as in the transport equations for k and ε. In these approaches, k and ε need to be interpreted as the subscale (or unresolved) turbulent kinetic energy and its dissipation rate. A potential inconsistency that arises from using a subscale k–ε model in PRNS arises from the fact this model generally uses the same values for the turbulence closure coefficients as was used for URANS k–ε model (in which no scales of turbulence are explicitly resolved). More specifically, when F_R is smaller than unity implying that some scales of the turbulence are resolved in the simulation, the closure coefficients in the subscale k–ε model need to be re-calibrated in order to reflect this change. In contrast, in our proposed PRNS approach, the eddy viscosity used to determine the turbulence diffusion and production terms of the k- and ε-transport equations [cf. (6) and (7)] is based on ν_t^{RANS} rather than ν_t^{PRNS}. In consequence, the k and ε quantities used in our current PRNS approach should be interpreted as (estimates of) "RANS" quantities, which are subsequently used to determine the integral length scale l_i required in our F_R formulation [cf. (17), (18), and (21)]. From this perspective, the use of conventional RANS values for the turbulence closure coefficients in the k–ε model is justifiable.

The PANS approach proposed by Girimaji [13] differs from other PRNS approaches, including our current PRNS formulation. In the PANS approach, no explicit F_R was needed to modify the eddy-viscosity owing to the fact that the k and ε quantities here are subscale (or unresolved) turbulent kinetic energy and its dissipation rate. Furthermore, Lakshmipathy and Girimaji [17] re-calibrated the values for the turbulence closure coefficients in their transport equation for the subscale k and ε by incorporating a viscosity reduction factor R (or, equivalently, F_R, in our current parlance). Lakshmipathy and Girimaji advocated using a constant value for R in order to minimize the influence of commutation errors. However, we argue that R needs to be "sensitized" to the local grid size, so that the model can determine the range of turbulence scales that are resolved and modeled in any particular region of the inhomogeneous flow for the given grid used.

Finally, we will provide some remarks concerning commutation errors. Wall functions are used for the near-wall modeling in our current PRNS approach. In consequence, our formulation for F_R forces PRNS to function as a RANS model near a solid surface, as is clearly evident from Fig. 5 (which will be discussed in "Section 4.1") where it is seen that F_R increases as the wall is approached. Since there are no commutation errors in RANS models, we expect that commutation errors associated with using an inhomogeneous spatial filter width (near the wall) may not be too significant for the results presented in this paper. However, because no explicit (discrete) filter operator is applied in most PRNS approaches (including the approach advocated in this paper), it is difficult to quantify the commutation errors in the simulation. Even so, there is no definitive evidence that the performance of simulations based on explicit filtering is necessarily better than those based on implicit filtering [3].

3 Numerical Details

The filtered Navier–Stokes equation was solved numerically using a collocated, finite-volume method based on the STREAM code [21]. The diffusive volume-face fluxes were discretized using a second-order accurate central differencing scheme

(CDS), whereas the convective volume-face fluxes were approximated using either a second-order accurate UMIST scheme [22] for the URANS calculations or a CDS for the PRNS and LES simulations. The transient term was discretized using a fully implicit, second-order accurate three-time-level method described in Ferziger and Peric [11]. The SIMPLE algorithm [30] was used to determine the pressure corrections. A nonlinear interpolation scheme [33] was used to interpolate the cell face velocities from the nodal velocities at the cell centers, in order to prevent checkerboard oscillations from developing in the pressure field.

The standard k–ε turbulence model was used for both the URANS and PRNS calculations, whereas the standard Smagorinsky model was used for LES. Periodic boundary conditions were applied in both the streamwise and spanwise directions. Wall functions were utilized at every solid boundary (e.g., channel walls, cube faces, etc.) to reduce the computational cost in the near-wall regions. Wall functions for the high-Re number k–ε model, described in Versteeg and Malalasekera [47], were used for URANS and PRNS. A wall stress model, based on the law-of-the-wall relationship, was used for LES:

$$\frac{\overline{u}}{u_\tau} = \frac{1}{\kappa_v} \ln\left(\frac{y u_\tau}{\nu}\right) + B, \tag{22}$$

where u_τ is the friction (shear) velocity, $\kappa_v = 0.41$ is the von Karman constant, and $B = 5.5$.

4 Results and Discussion

For each test case, computations from URANS, PRNS and LES were performed using the same mesh size. All results presented were averaged in time, and the angled brackets surrounding a quantity are used to denote the time average of that quantity. The Reynolds stresses (obtained from time-averaging of the product of various fluctuating velocities) are calculated from the relationship

$$\overline{u_i' u_j'} = \left\langle u_i'' u_j'' \right\rangle + \langle \tau_{ij} \rangle, \tag{23}$$

where $\left\langle u_i'' u_j'' \right\rangle \equiv \langle \overline{u}_i \overline{u}_j \rangle - \langle \overline{u}_i \rangle \langle \overline{u}_j \rangle$ and $\langle \tau_{ij} \rangle$ are the resolved and modeled components of Reynolds stresses, respectively. The resolved Reynolds stresses represent the contribution arising from the resolved fluctuating velocity field (which can be computed directly). Note that $\left\langle u_i'' u_j'' \right\rangle = 0$ if a RANS calculation is performed, and in this case (23) reduces to $\overline{u_i' u_j'} = \tau_{ij}^{RANS}$ which is consistent with (4).

4.1 Plane channel flow

The DNS data of Moser et al. [26] for a fully-developed turbulent plane channel flow at $Re_\tau \equiv \delta u_\tau / \nu = 590$ was taken as the benchmark test case (δ is the channel half width). This data was generated using $384 \times 257 \times 384$ nodes in a computational domain with a physical extent of $L_x \times L_y \times L_z = 2\pi\delta \times 2\delta \times \pi\delta$ in the streamwise (x), wall-normal (y) and spanwise (z) directions, respectively. The current simulations used a uniform mesh of $(N_x, N_y, N_z) = (46, 46, 46)$ cells for a computational domain having the same physical size as that used for the DNS study. For the plane channel

flow simulation, statistics of the flow were obtained by averaging over a horizontal plane parallel to the channel wall and in time.

Figure 2 shows the mean streamwise velocity profiles (expressed in wall units) obtained from URANS, PRNS and LES. In general, the URANS predictions of the mean streamwise velocity are in good conformance with the logarithmic law-of-the-wall relationship. However, the PRNS and LES results exhibit a velocity shift, which starts at the second node from the wall. Furthermore, the velocity gradients for PRNS and LES, as determined by the first few nodes from the wall, are too large in comparison with the DNS result. It should be noted that this shift in the mean streamwise velocity profile has been observed in various flow simulation approaches, including LES applied with wall models [2, 4], zonal hybrid RANS/LES [45, 46] and DES [29, 32]. The primary cause of this velocity shift is the generation of an artificial buffer layer that develops at a location between the near-wall and outer regions of the flow, where the simulation experiences a transition from a region where the turbulence is largely modeled to one where it is largely resolved.

It can be shown that the mean velocity gradient for a fully-developed plane channel flow can be expressed as

$$\frac{\partial \langle \tilde{u} \rangle}{\partial y} \approx \frac{u_\tau^2 \left(1 - y/\delta\right) - \left\langle -u''v'' \right\rangle}{\nu + \langle \nu_t \rangle}, \tag{24}$$

where $\langle u''v'' \rangle$ is the resolved turbulent shear stress. Equation (24) suggests that the velocity gradient is related to the resolved shear stress and the eddy viscosity. Owing to the coarse grid used in the near-wall region in our simulations, the resolved turbulent shear stress at the first few nodes above the wall in PRNS and LES is under-predicted (see Fig. 3), yielding a steeper velocity gradient at these nodes because the value of numerator on the right-hand-side of (24) is over-predicted. In the core region of the plane channel where the turbulence is mostly resolved, the velocity profiles of PRNS and LES in this region have approximately the same slope as the DNS results (cf. Fig. 2), except that the values of the $\langle u^+ \rangle$-intercept [i.e., B in (22)] as predicted by PRNS and LES are larger than that obtained with DNS owing to the velocity shift.

Figure 4 displays profiles of the eddy or subscale viscosity (normalized by the molecular viscosity). Since the eddy viscosity is related to the modeled turbulence, the magnitude of the eddy viscosity for URANS is the greatest among the three simulations because turbulence in URANS is mostly modeled. In contrast, the (SGS) eddy viscosity for LES has the smallest value because only the smallest scales

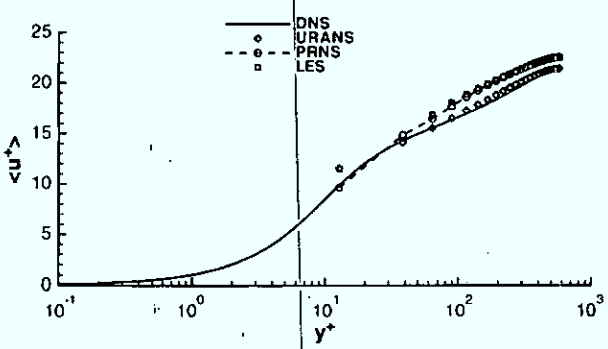

Fig. 2 Mean velocity profiles for a plane channel flow

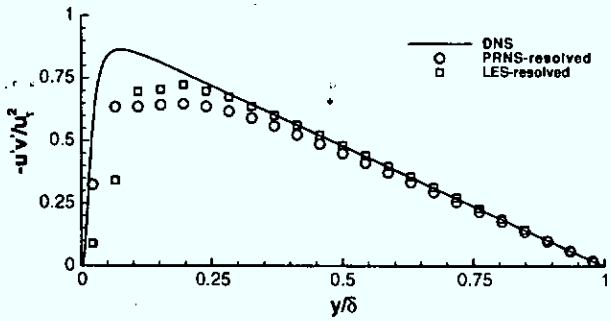

Fig. 3 Reynolds shear stress profiles for a plane channel flow

of turbulence (which are not resolved in the simulation) are modeled here. The (subscale) eddy viscosity for PRNS [cf. (14)] is calculated as $\nu_t^{PRNS} = F_R C_\mu k^2/\varepsilon$ [viz., this is the eddy viscosity which is used to compute the turbulent stresses in the filtered momentum equation]. The distribution of F_R is shown in Fig. 5, where it is seen that the value of F_R gradually decreases away from the wall. A smaller value of F_R implies that a greater fraction of the scales of turbulence is resolved. It can be seen from Fig. 3 that a significant portion of the turbulent shear stress in PRNS is resolved in the core region of the plane channel.

If the first grid node from the wall lies in the log-law layer, an analytical value of F_R at this node can be estimated using the log-law relationship for k and ε:

$$k = C_\mu^{-1/2} u_\tau^2, \ \varepsilon = u_\tau^3/\kappa_v y. \tag{25}$$

Substituting (25) into (21) yields

$$(l_i, l_c, l_\kappa) = \left[C_\kappa \kappa_v C_\mu^{-3/4} y_P, 2\left(\Delta_x \Delta_y \Delta_z\right)^{1/3}, \kappa_v^{1/4} y_P^{1/4} Re_\tau^{-3/4} \delta^{3/4}\right], \tag{26}$$

where $y_P = 0.5\Delta_y$ is the normal distance to the wall from the first off-wall node. The grid spacing in the three coordinate directions is determined as

$$\left(\Delta_x, \Delta_y, \Delta_z\right) = \left(L_x/N_x, L_y/N_y, L_z/N_z\right), \tag{27}$$

based on the values for (L_x, L_y, L_z) and (N_x, N_y, N_z) mentioned earlier. With the values of $\kappa_v = 0.41$, $C_\kappa = 40$ and $\mathrm{Re}_\tau = 590$, $F_R \approx 0.16$ is obtained from (17), using

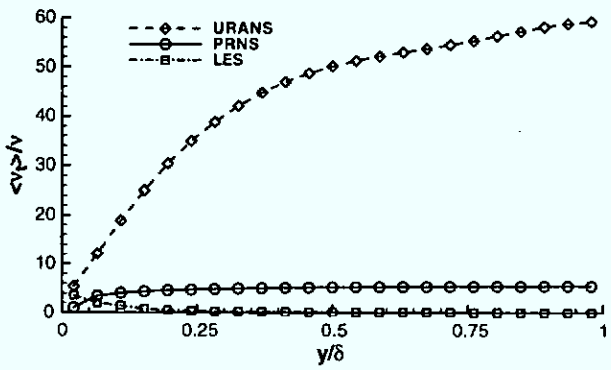

Fig. 4 Mean eddy viscosity profiles for a plane channel flow

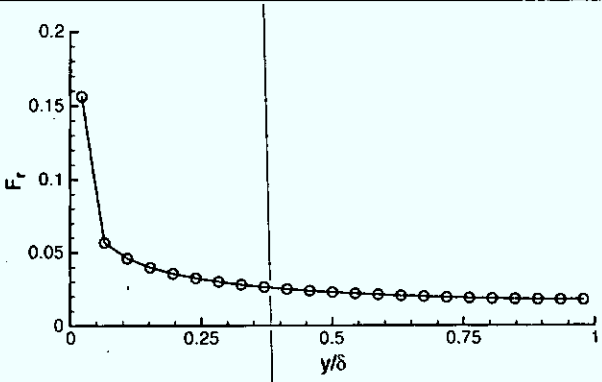

Fig. 5 Resolution control function profile for a plane channel flow

the values for the various wave numbers, length scales, and grid spacings calculated from (18), (26) and (27). This analytical value of F_R is consistent with the computed value at the first node from the wall shown in Fig. 5. Similarly, a lower bound value of C_κ can be obtained by setting $l_e = l_t$ [which yields $F_R = 1$ in (17)]. This leads to

$$C_\kappa^{\min} = \frac{4\left(\Delta_x \Delta_y \Delta_z\right)^{1/3} C_\mu^{3/4}}{\kappa_v \Delta_y} \approx 2.67. \tag{28}$$

However, we note that this value for $C_\kappa^{\min}$ (for the given mesh size used here) yielded a subscale eddy viscosity (i.e., $\nu_t^{PRNS} = F_R \nu_t$) that was too large and hence too dissipative, resulting in the damping of all the turbulent velocity fluctuations in the channel flow (at $\mathrm{Re}_\tau = 590$). It was found that when the value of C_κ was increased to ≈ 40, the excessive damping of the large-scale turbulent fluctuations in the flow did not occur and PRNS behaved like VLES in this case (rather than RANS).

Predictions of the root-mean-square (rms) velocity ($u'_{i,rms} \equiv \sqrt{\overline{u'_i u'_i}}$, with no implied summation on the repeated index i) profiles provided by URANS, PRNS, and LES are compared with the DNS results in Fig. 6. While DNS shows strong anisotropic rms velocities (with $u'_{rms} > w'_{rms} > v'_{rms}$), the predictions provided by URANS give isotropic rms velocities (i.e., $u'_{i,rms} = \sqrt{2k/3}$) owing to the use of the linear Boussinesq stress-strain relationship [cf. (4)] in which $\overline{S}_{11} = \overline{S}_{22} = \overline{S}_{33} = 0$ for the fully-developed channel flow. LES provides improved predictions of the near-wall anisotropic rms velocities compared to URANS, but it over-estimates u'_{rms} and under-estimates v'_{rms} and w'_{rms}. In addition, the location and magnitude of the peak of u'_{rms} is incorrect. These problems (known to occur for coarse-grid LES used with wall function models) have also been reported by Cabot and Moin [4] and Benarafa et al. [2]. PRNS provides predictions of v'_{rms} and w'_{rms} that conform reasonably well with the DNS results. As in the case of LES, PRNS over-estimates u'_{rms} and provides an incorrect location for the peak of u'_{rms}. The location of the maximum of u'_{rms} occurs at $y^+ = 14$ (or $y/\delta = 0.024$) in the DNS results (cf. Fig. 6). This location lies within the physical buffer layer ($5 < y^+ < 30$), and coincides with the location of the maximum in the turbulence energy production (i.e., $-\overline{u'v'}\partial\overline{u}/\partial y$). Because the near-wall eddies are responsible for a major portion of the turbulence energy production, these small scales of motion must be well resolved in order to provide accurate results. Using a computational grid that is too coarse to resolve these eddies generally results in poor

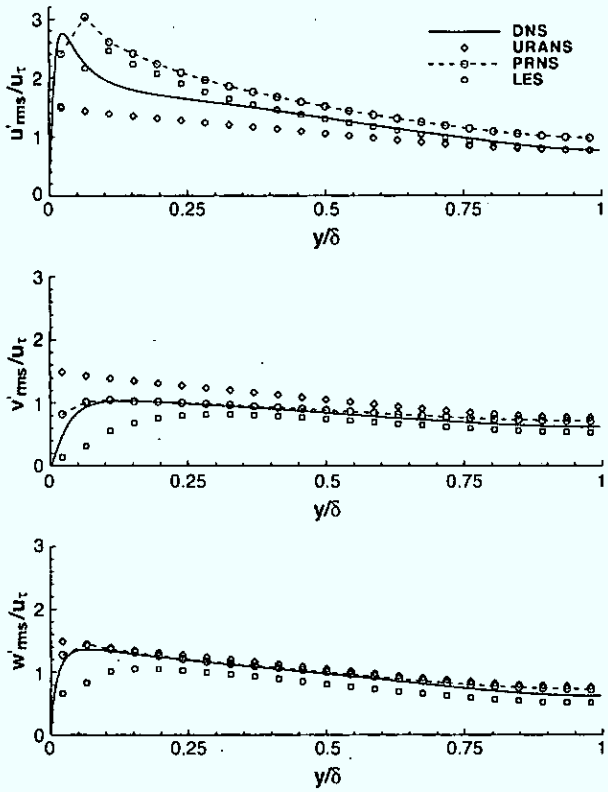

Fig. 6 Root-mean-square velocity profiles for a plane channel flow

predictions of the rms velocities. In addition, any simulation that uses wall functions is unable to capture the correct location of the peak u'_{rms} which occurs within the buffer layer, since the first near-wall node used in the wall function approach is placed (ideally) at $y^+ > 30$ outside the buffer layer.

4.2 Flow over a matrix of cubes

The test case considered here is the wind tunnel experiment of Meinders and Hanjalic [25], which was used as one of the benchmark problems in the Eighth European Research Community on Flow, Turbulence and Combustion (ERCOFTAC) workshop on turbulence modeling [16]. The experiment consisted of the measurement of the flow in an extensive array of 250 cubes (25 rows of ten equally spaced cubes) placed in a plane channel flow. Velocity measurements were made around the 18th row in the array of cubes, near the centerline of the plane channel. The flow at this location was fully developed, and as a consequence periodic boundary conditions can be applied in both the streamwise and spanwise directions for the flow simulation.

Figure 7 shows the geometry of the cubical array. The heights of each cube and the channel were H and $3.4H$, respectively. The separation between the cubes (face-to-face) in both the streamwise and spanwise directions was $3H$. The Reynolds number, based on the cube height and bulk velocity (U_b), was 3,854. All computations were performed on a mesh of $49 \times 49 \times 49$ nodes in a computational domain that consisted

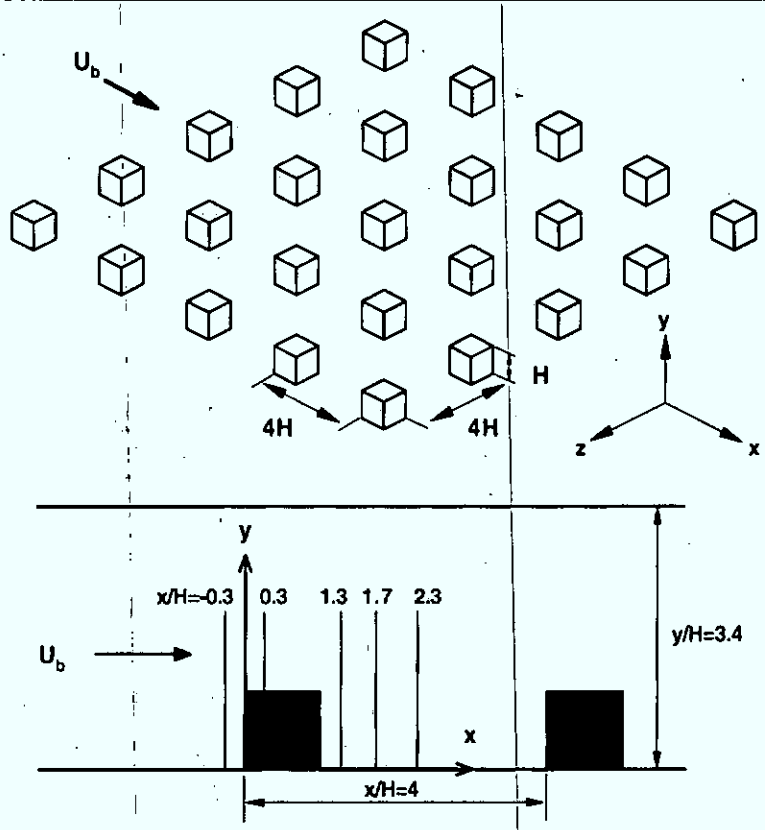

Fig. 7 The geometry of an array of cubes and a side view of a sub-channel unit cell showing the locations of the velocity measurements

of a sub-channel unit cell of dimensions of $4H \times 3.4H \times 4H$ in the streamwise (x), wall-normal (y) and spanwise (z) directions, respectively. Predicted results from the simulation were compared with the experimental data at four selected locations (namely, at $x/H = -0.3$, 0.3, 1.3 and 1.7) displayed in Fig. 7.

The mean velocity vector fields in the vertical x–y plane at $z/H = 0$ and the horizontal x–z plane at $y/H = 0.5$, predicted using URANS, PRNS and LES, are shown in Figs. 8 and 9, respectively. It can be seen that all approaches are capable of capturing the various flow structures such as the separation at the sharp leading top and side edges of the cube (at $x/H \doteq 0$) and the recirculation zone in the wake region behind the cube. Figure 8 exhibits a two-cell vortex structure in the street canyons: namely, a downward vortex and an upward arch vortex on the windward and leeward faces of the cube, respectively. In the LES study of Niceno et al. [28], they observed a stagnation point (caused by the flow impingement) located at $y/H \approx 0.8$ and $y/H \approx 0.25$ on the windward and leeward faces of cube, respectively. Similar locations for a stagnation point were found in the current study, except for URANS whose predictions do not exhibit a stagnation point on the leeward face of the cube. It can be seen in Fig. 8 that the flow predicted by URANS exhibits only upward velocities along the leeward face of the cube, which contrasts sharply with the PRNS

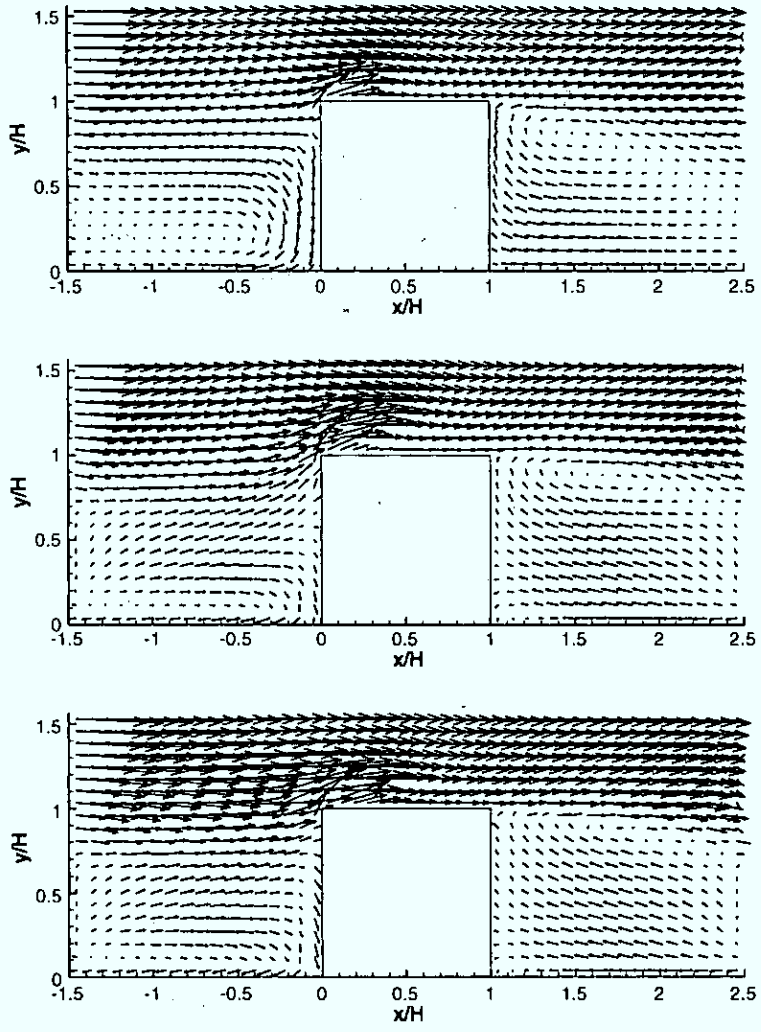

Fig. 8 Mean velocity vector field in the vertical x–y plane at $z/H = 0$ obtained using URANS (*top*), PRNS (*middle*) and LES (*bottom*)

and LES results where the flow is seen to exhibit downward velocities below the stagnation point at $y/H \approx 0.3$.

Figure 9 demonstrates that the mean flow is symmetrical along the centerline at $z/H = 0$. The flow is mostly undisturbed in the spanwise corridor region between two cubes. Two small separation bubbles on the side faces of the cube are observed. A pair of counter-rotating vortices in the wake region is evident. The center of these vortices for URANS is located at $x/H \approx 1.4$, in contrast with those for PRNS and LES where the center of the vortices are seen to be located at $x/H \approx 1.7$.

Figure 10 shows the mean streamwise velocity predictions in the vertical x–y plane at $z/H = 0$ and in the horizontal x–z plane at $y/H = 0.5$. While the mean velocity profiles in the $z/H = 0$ plane obtained using the three approaches are generally

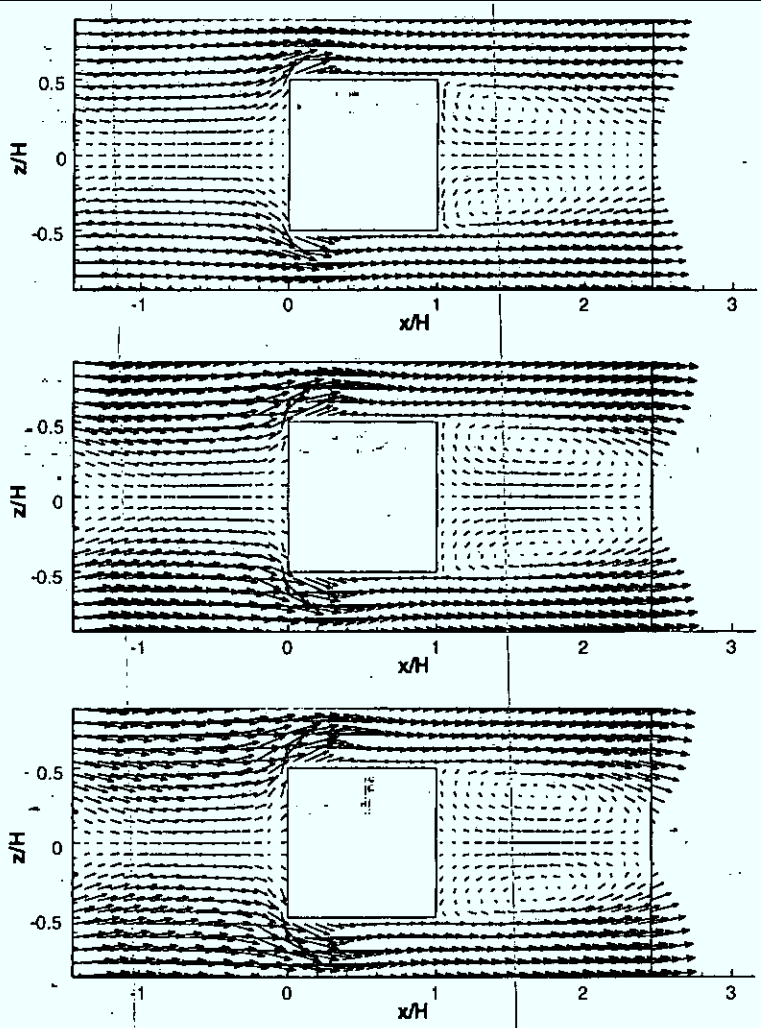

Fig. 9 Mean velocity vector field in the horizontal x–z plane at $y/H = 0.5$ obtained using URANS (*top*), PRNS (*middle*) and LES (*bottom*)

similar as evident from Fig. 10a, it is found that LES gives the best conformance with the experimental data. URANS agrees with the experimental measurements reasonably well for $y/H > 1$ where the flow is attached, but shows visible discrepancies within the recirculation zone ($y/H < 1$) in the lee of the cube, where the flow exhibits reversals at the streamwise locations $x/H = -0.3$, 1.3 and 1.7. In contrast, PRNS under-predicts the velocity in the region $1 < y/H < 2.5$. Similar under-predictions of the velocity in this region were found in the LES results reported by Niceno and

Fig. 10 Profiles of mean streamwise velocity in **a** the vertical x–y plane at $z/H = 0$ and **b** the ▶ horizontal x–z plane at $y/H = 0.5$

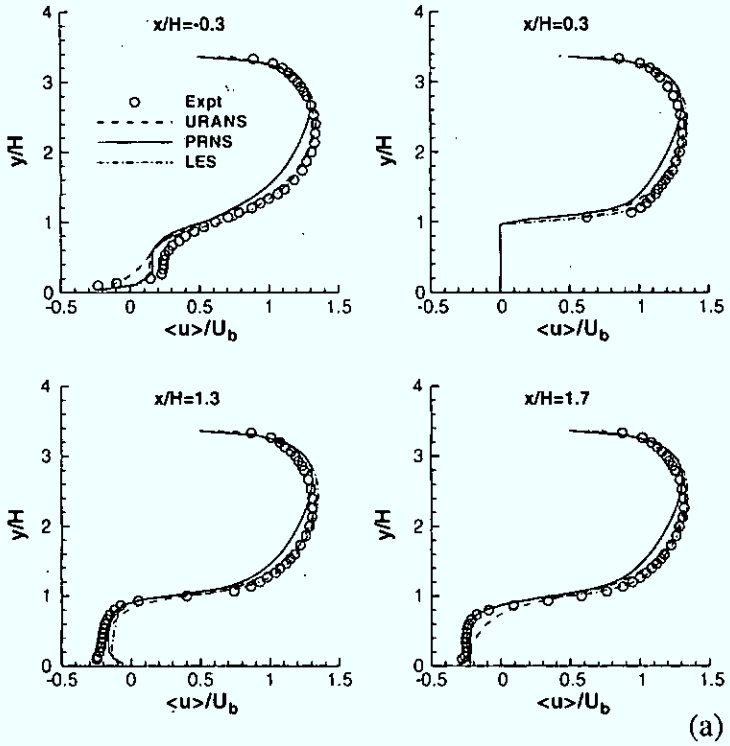
x/H=-0.3
x/H=0.3
x/H=1.3
x/H=1.7
Expt
URANS
PRNS
LES
y/H
<u>/U_b

(a)

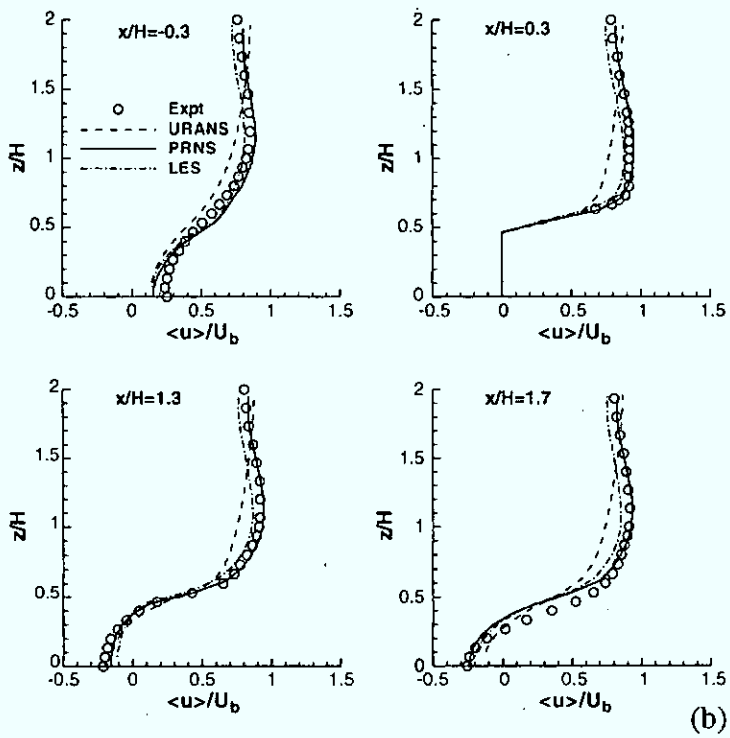
x/H=-0.3
x/H=0.3
x/H=1.3
x/H=1.7
Expt
URANS
PRNS
LES
z/H
<u>/U_b

(b)

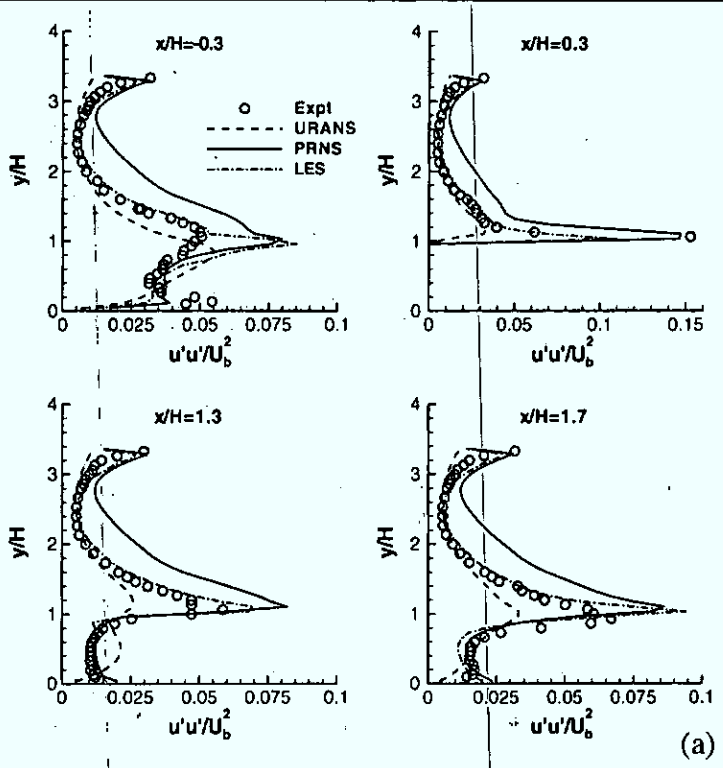
x/H=-0.3
x/H=0.3
x/H=1.3
x/H=1.7
Expt
URANS
PRNS
LES
y/H
u'u'/U_b^2

(a)

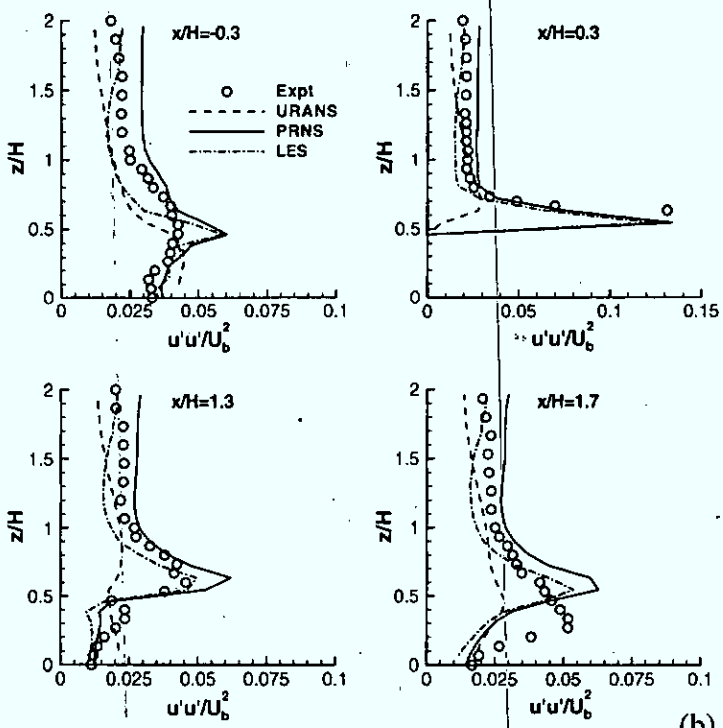
x/H=-0.3
x/H=0.3
x/H=1.3
x/H=1.7
Expt
URANS
PRNS
LES
z/H
u'u'/U_b^2

(b)

◀ **Fig. 11** Profiles of streamwise Reynolds normal stress in **a** the vertical x–y plane at $z/H = 0$ and **b** the horizontal x–z plane at $y/H = 0.5$

Hanjalic [27]. The PRNS results provide slightly better predictions of the reverse flow within the recirculation zone than the LES results. Figure 10b shows that both PRNS and LES capture the correct shape of the mean streamwise velocity profiles in the x–z plane at $y/H = 0$, but PRNS agrees better with the experimental data than LES. In contrast, predictions from URANS provide erroneous velocity profiles in the spanwise corridor region between two cubes for $z/H > 0.5$. The predicted velocity in URANS increases monotonically in the region $0.5 < z/H < 2$, which is contradictory to the measured velocity which is seen to increase for $0.5 < z/H < 1$ and then decrease for $1 < z/H < 2$.

Comparison of the measured and predicted streamwise Reynolds normal stresses $\overline{u'u'}$ are presented in Fig. 11. Note that the peak value of $\overline{u'u'}$ at each x-location occurs at $y/H \approx 1$ in the $z/H = 0$ plane and at $z/H \approx 0.5$ in the $y/H = 0.5$ plane. These peaks in $\overline{u'u'}$ correspond to the development of the thin shear layers along the rooftop and side walls of the cube, respectively. These shear layers originate from the sharp leading edges of the cube, and result in strong velocity gradients that contribute to a significant production (generation) of $\overline{u'u'}$ (viz., through the production term $-2\overline{u'_1u'_k}\partial\overline{u}_1/\partial x_k$ where $\overline{u}_1 \equiv \overline{u}$). Moreover, the maximum value of $\overline{u'u'}$ is found within the thin separation zone (i.e., at $x/H = 0.3$), where a large streamwise velocity gradient $\partial\overline{u}/\partial x$ occurs as a result of the separation of the shear layer and its subsequent reattachment.

In terms of the shape and magnitude of the $\overline{u'u'}$ profiles, discrepancy between the URANS results and the experimental data is generally quite large. In particular, URANS significantly under-estimates the peak value of $\overline{u'u'}$ by more than 50% at the streamwise locations $x/H = 0.3$, 1.3 and 1.7. This under-prediction of the streamwise Reynolds normal stress in URANS arises from the utilization of the linear Boussinesq stress–strain relationship [cf. (4)], which cannot properly account for the effects of anisotropy in the Reynolds stresses. In contrast, the LES results are in fairly good agreement with the experimental measurements in the $z/H = 0$ plane, but these predictions moderately under-predict the magnitude of $\overline{u'u'}$ in the $y/H = 0.5$ plane. Finally, the PRNS results give predictions for $\overline{u'u'}$ that are similar to those provided by the LES results, but PRNS is observed to over-estimate the magnitude of $\overline{u'u'}$ for $y/H > 1$ [see Fig. 11a] and for $z/H > 0.5$ [see Fig. 11b]. The over-prediction of $\overline{u'u'}$ in these regions was also reported in the DES study of Schmidt and Thiele [35], where their grid size (≈120,000 cells) was similar to our current grid size of $49^3 (= 117,649)$ nodes. However, their predictions of the values for $\overline{u'u'}$ were generally larger than our current PRNS predictions by at least a factor of two.

Profiles of the spanwise Reynolds normal stress $\overline{w'w'}$ are exhibited in Fig. 12. From Fig. 12a, it is seen that the peak value of $\overline{w'w'}$ at each x-location occurs at $y/H \approx 1$ in the $z/H = 0$ plane. Large values of $\overline{w'w'}$ are also observed in the range $0.2 < y/H < 0.8$ at $x/H = -0.3$, which are associated with the flow impingement on the windward face of the cube. Within this impingement zone, the maximum value of $\overline{w'w'}$ in the x–z plane at $y/H = 0.5$ is found to occur at the centerline $z/H = 0$ [cf. Fig. 12b], corresponding to the existence of a large spanwise velocity gradient $\partial\overline{w}/\partial z$ which results in a significant production of $\overline{w'w'}$ (through the production term

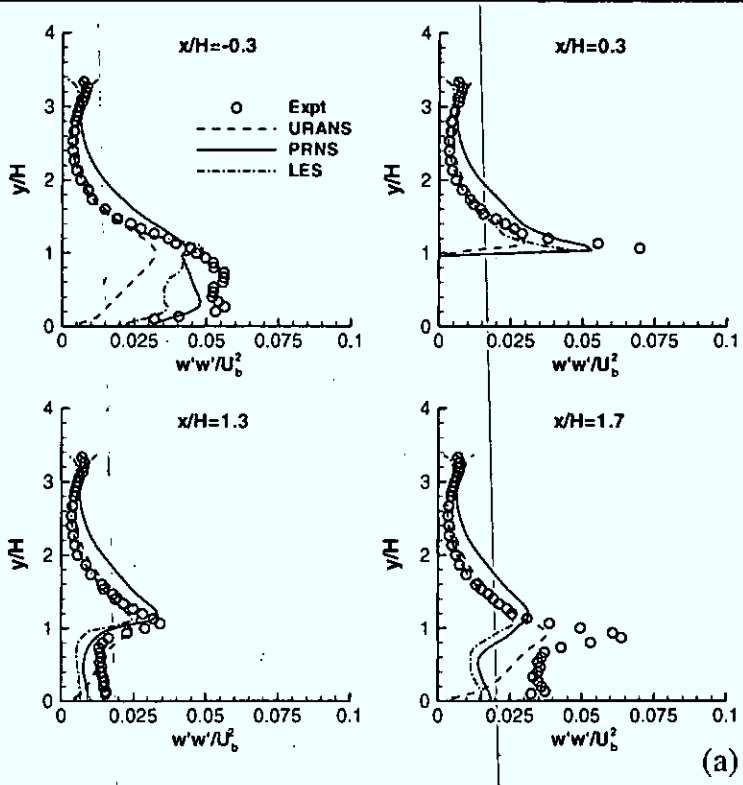
x/H=-0.3
x/H=0.3
x/H=1.3
x/H=1.7
Expt
URANS
PRNS
LES
y/H
w'w'/U_b^2
0
0.025
0.05
0.075
0.1
1
2
3
4

(a)

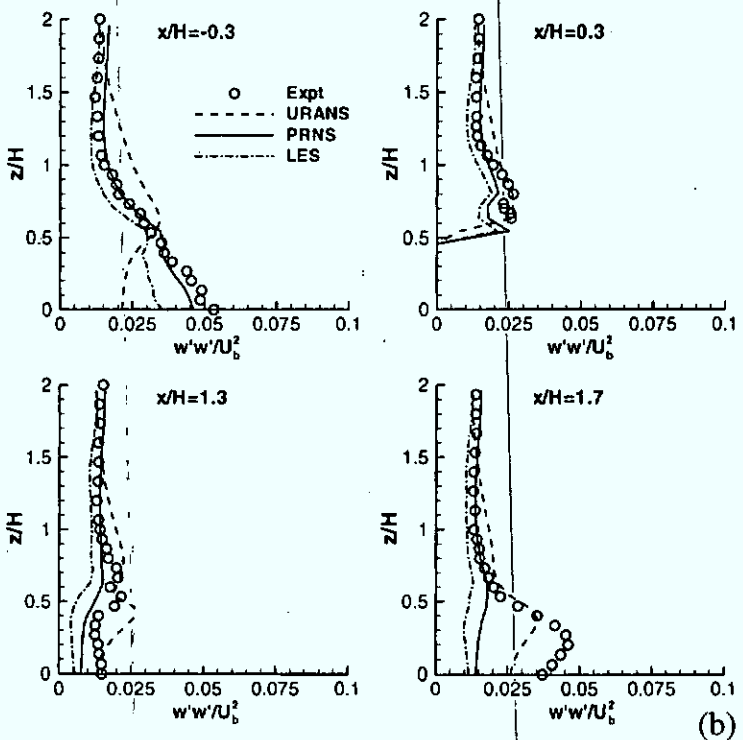
x/H=-0.3
x/H=0.3
x/H=1.3
x/H=1.7
Expt
URANS
PRNS
LES
z/H
w'w'/U_b^2
0
0.025
0.05
0.075
0.1
0.5
1
1.5
2

(b)

◀ **Fig. 12** Profiles of spanwise Reynolds normal stress in **a** the vertical x–y plane at $z/H = 0$ and **b** the horizontal x–z plane at $y/H = 0.5$

$-2\overline{u_3'u_k'}\partial\bar{u}_3/\partial x_k$ where $\bar{u}_3 \equiv \bar{w}$). In contrast, the magnitude of $\overline{w'w'}$ near the leeward face of the cube at $x/H = 1.3$ for $z/H < 0.5$ is relatively small.

The URANS predictions for $\overline{w'w'}$ are generally poor, except in the x–y plane at $z/H = 0$ for $y/H > 1$ [see Fig. 12a]. In contrast, a good conformance of PRNS and LES predictions with the experimental results is obtained. In particular, the shapes of the $\overline{w'w'}$ profiles are fairly well captured. However, both the PRNS and LES results significantly under-estimate the magnitude of $\overline{w'w'}$ at $x/H = 1.3$ and 1.7 for $y/H < 1$ [cf. Fig. 12a] and for $z/H < 0.5$ [cf. Fig. 12b]. The large discrepancy in the predictions of the values of $\overline{w'w'}$ in these regions was also reported by Cheng

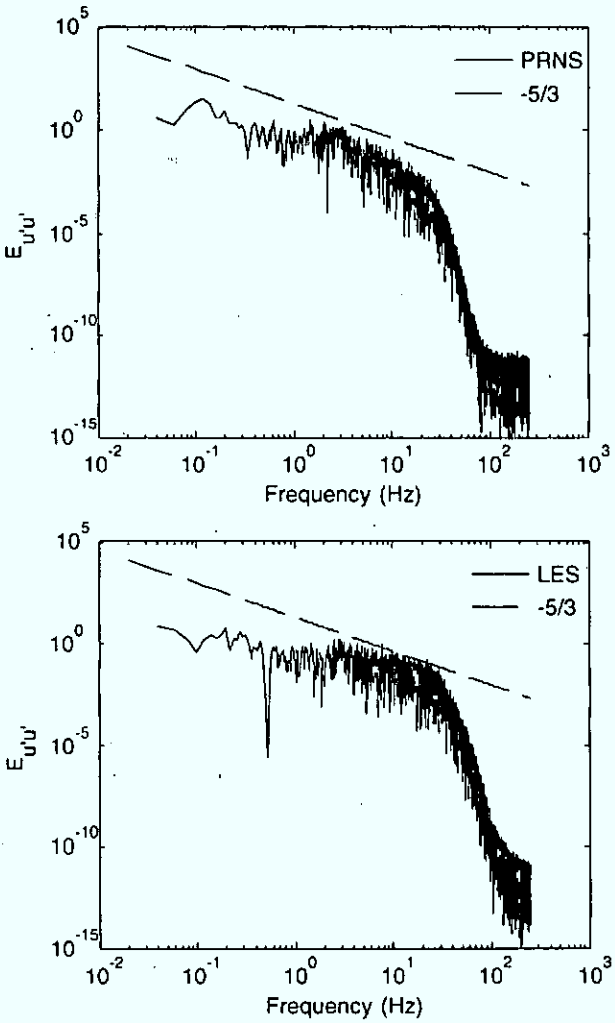

Fig. 13 Time energy spectra obtained from PRNS (*top*) and LES (*bottom*) for the streamwise velocity at $(x/H, y/H, z/H) = (0.5, 1.3, 0)$

et al. [5], whose numerical study included LES with the standard Smagorinsky model and two different dynamic SGS stress models. Note that Cheng et al. [5] performed LES on a staggered grid using a numerical scheme, which discretely conserves mass, momentum, and kinetic energy (in the inviscid limit) in both space and time [15]. In contrast, a collocated grid is used in the present study.

Figure 13 shows the energy spectrum obtained from PRNS and LES for the streamwise velocity at location $(x/H,\ y/H,\ z/H) = (0.5,\ 1.3,\ 0)$. According to Kolmogorov theory, the energy spectrum of a high Reynolds-number flow normally exhibits a $-5/3$ slope in the inertial subrange. The energy spectra predicted by LES exhibits an inertial subrange spanning about one decade in the frequency range from about 3 Hz to about 30 Hz, which implies that LES adequately resolves most of the energy in the turbulent flow. In contrast, the energy spectra predicted by PRNS drops off more quickly than LES. This indicates that PRNS resolves less turbulence than LES, which is expected.

5 Conclusions

The concept of PRNS, along with various formulations for F_R, has been reviewed in this paper. Performance of PRNS, with a newly proposed functional form for F_R and used in conjunction with the standard k–ε model, is evaluated against URANS and LES for two different wall-bounded turbulent flows. For the simulation of a plane channel flow, the URANS predictions for the streamwise mean velocity agree well with the logarithmic law-of-the-wall relationship, whereas the PRNS and LES predictions exhibit a velocity shift (a common problem seen in many hybrid RANS/LES approaches and in LES used with wall models). However, the PRNS and LES predictions are able to capture the near-wall anisotropy in the rms velocities, whereas the URANS predictions cannot. It was found that PRNS and LES provided incorrect predictions for the location and magnitude of the peak in u'_{rms}. Nevertheless, the PRNS results gave the best overall conformance with the v'_{rms} and w'_{rms} profiles obtained from DNS.

For flow over an array of cubes, flow structures such as separation bubbles were captured reasonably well by all three simulation methodologies. The URANS results gave a poor conformance with the experimental data in general, particularly for the predictions of the Reynolds stresses within the recirculation zone in the lee of the cube. In contrast, PRNS and LES provided good predictions for the mean velocities and Reynolds stresses, both in terms of the shapes and magnitudes of the profiles.

Results for both test problems suggest that the predictive performance of PRNS, qualitatively and quantitatively, is comparable to that of LES. This study demonstrates the potential of applying PRNS to other more complex turbulent flows, such as a spatially developing flow over a built-up (urban) area, where other physical phenomena such as buoyancy-induced turbulence may be important as well.

Acknowledgements This work has been supported by Chemical Biological Radiological Nuclear Research and Technology Initiative (CRTI) program under project number CRTI-02-0093RD. The computations conducted in this study were made possible by the facilities of the Shared Hierarchical Academic Research Computing Network (SHARCNET).

References

1. Batten, P., Goldberg, U., Chakravarthy, S.: Interfacing statistical turbulence closures with large-eddy simulation. AIAA J. **42**, 485–492 (2004). doi:10.2514/1.3496
2. Benarafa, Y., Cioni, O., Ducros, F., Sagaut, P.: RANS/LES coupling for unsteady turbulent flow simulation at high Reynolds number on coarse meshes. Comput. Methods Appl. Mech. Eng. **195**, 2939–2960 (2006). doi:10.1016/j.cma.2005.06.007
3. Brandt, T.T.: Study of large eddy simulation and Smagorinsky model using explicit filtering. AIAA Paper 2006-3541 (2006)
4. Cabot, W., Moin, P.: Approximate wall boundary conditions in the large-eddy simulation of high Reynolds number flow. Flow Turbul. Combust. **63**, 269–291 (1999). doi:10.1023/A:1009958917113
5. Cheng, Y., Lien, F.-S., Yee, E., Sinclair, R.: A comparison of large-eddy simulations with a standard k–ε Reynolds-averaged Navier–Stokes model for the prediction of a fully developed turbulent flow over a matrix of cubes. J. Wind Eng. Ind. Aerodyn. **91**, 1301–1328 (2003). doi:10.1016/j.jweia.2003.08.001
6. Davidson, L., Billson, M.: Hybrid LES-RANS using synthesized turbulent fluctuations for forcing in the interface region. Int. J. Heat Fluid Flow **27**, 1028–1042 (2006). doi:10.1016/j.ijheatfluidflow.2006.02.025
7. Davidson, L., Dahlstrom, S.: Hybrid LES-RANS: an approach to make LES applicable at high Reynolds number. Int. J. Comput. Fluid Dyn. **19**, 415–427 (2005). doi:10.1080/10618560500242280
8. Davidson, L., Peng, S.H.: Hybrid LES-RANS modeling: a one-equation SGS model combined with a k–ω model for predicting recirculating flows. Int. J. Numer. Methods Fluids **43**, 1003–1018 (2003). doi:10.1002/fld.512
9. Deardorff, J.W.: A numerical study of three-dimensional turbulent channel flow at large Reynolds numbers. J. Fluid Mech. **41**, 453–480 (1970). doi:10.1017/S0022112070000691
10. Fasel, H.F., Seidel, J., Wernz, S.: A methodology for simulations of complex turbulent flows. J. Fluids Eng. **124**, 933–942 (2002). doi:10.1115/1.1517569
11. Ferziger, J.H., Peric, M.: Computational Methods for Fluid Dynamics. Springer, Berlin (2002)
12. Germano, M., Piomelli, U., Moin, P.: A dynamic subgrid-scale eddy viscosity model. Phys. Fluids, A **3**, 1760–1765 (1991). doi:10.1063/1.857955
13. Girimaji, S.S.: Partially-averaged Navier–Stokes model for turbulence: a Reynolds-averaged Navier–Stokes to direct numerical simulation bridging method. J. Appl. Mech. **73**, 413–421 (2006). doi:10.1115/1.2151207
14. Grotzbach, G.: Direct numerical and large-eddy simulation of turbulent channel flows. In: Cheremisinoff, N.P. (ed.) Encyclopedia of Fluid Mechanics, vol. 6. Gulf, Houston (1987)
15. Ham, F.E., Lien, F.S., Strong, A.B.: A fully conservative second-order finite difference scheme for incompressible flow on nonuniform grids. J. Comput. Phys. **177**, 117–133 (2002). doi:10.1006/jcph.2002.7006
16. Hellsten, A., Rautaheimo, P. (eds.): Proceedings of the 8th ERCOFTAC/IAHR/COST Workshop on Refined Turbulence Modeling, Helsinki, Finland (1999)
17. Lakshmipathy, S., Girimaji, S.S.: Extension of Boussinesq turbulence constitutive relation for bridging methods. J. Turbul. **8**(31), 1–21 (2007). doi:10.1080/14685240701420478
18. Larsson, J., Lien, F.S., Yee, E.: Feedback-controlled forcing in hybrid LES/RANS. Int. J. Comput. Fluid Dyn. **20**, 687–699 (2006). doi:10.1080/10618560701214724
19. Larsson, J., Lien, F.S., Yee, E.: The artificial buffer layer and the effect of forcing in hybrid LES/RANS. Int. J. Heat Fluid Flow **28**, 1443–1459 (2007). doi:10.1016/j.ijheatfluidflow.2007.04.007
20. Launder, B.E., Spalding, D.B.: The numerical computation of turbulent flows. Comput. Methods Appl. Mech. Eng. **3**, 269–289 (1974). doi:10.1016/0045-7825(74)90029-2
21. Lien, F.S., Leschziner, M.A.: A general non-orthogonal collocated finite volume algorithm for turbulent flow at all speeds incorporating second-moment closure, part 1: numerical implementation. Comput. Methods Appl. Mech. Eng. **114**, 123–148 (1994). doi:10.1016/0045-7825(94)90165-1
22. Lien, F.S., Leschziner, M.A.: Upstream monotonic interpolation for scalar transport with application in complex turbulent flows. Int. J. Numer. Methods Fluids **19**, 527–548 (1994). doi:10.1002/fld.1650190606
23. Lilly, D.K.: The representation of small-scale turbulence in numerical simulation experiments. In: Proceedings of the IBM Scientific Computing Symposium on Environmental Sciences, Yorktown Heights, USA (1967)

24. Liu, N.-S., Shih, T.-H.: Turbulence modeling for very large-eddy simulation. AIAA J. **44**, 687–697 (2006). doi:10.2514/1.14452
25. Meinders, E.R., Hanjalic, K.: Vortex structure and heat transfer in turbulent flow over a wall-mounted matrix of cubes. Int. J. Heat Fluid Flow **20**, 255–267 (1999). doi:10.1016/S0142-727X(99)00016-8
26. Moser, R.D., Kim, J., Mansour, N.N.: Direct numerical simulation of turbulent channel flow up to $Re_\tau = 590$. Phys. Fluids **11**, 943–945 (1999). doi:10.1063/1.869966
27. Niceno, B., Hanjalic, K: Flow in a matrix of surface-mounted cubes—test case 6.2: description of numerical methodology. In: Proceedings of the 8th ERCOFTAC/IAHR/COST Workshop on Refined Turbulence Modeling, Helsinki, Finland (1999)
28. Niceno, B., Dronkers, A.D.T., Hanjalic, K.: Turbulent heat transfer from a multi-layered wall-mounted cube matrix: a large-eddy simulation. Int. J. Heat Fluid Flow **23**, 173–185 (2002). doi:10.1016/S0142-727X(01)00147-3
29. Nikitin, N.V., Nicoud, F., Wasistho, B., Squires, K.D., Spalart, P.R.: An approach to wall modeling in large-eddy simulations. Phys. Fluids **12**, 1629–1632 (2000). doi:10.1063/1.870414
30. Patankar, S.V., Spalding, D.B.: A calculation procedure for heat, mass and momentum transfer in three-dimensional parabolic flows. Int. J. Heat Mass Transfer **15**, 1787–1806 (1972). doi:10.1016/0017-9310(72)90054-3
31. Piomelli, U., Ferziger, J., Moin, P., Kim, J.: New approximate boundary conditions for large-eddy simulations of wall-bounded flows. Phys. Fluids, A **1**, 1061–1068 (1989). doi:10.1063/1.857397
32. Piomelli, U., Balaras, E., Pasinato, H., Squires, K.D., Spalart, P.R.: The inner–outer layer interface in large-eddy simulations with wall-layer models. Int. J. Heat Fluid Flow **24**, 538–550. (2003) doi:10.1016/S0142-727X(03)00048-1
33. Rhie, C.M., Chow, W.L.: Numerical study of the turbulent flow past an airfoil with trailing edge separation. AIAA J. **21**, 1525–1532 (1983). doi:10.2514/3.8284
34. Sagaut, P.: Large Eddy Simulation for Incompressible Flows. Springer, Heidelberg (1998)
35. Schmidt, S., Thiele, F.: Comparison of numerical methods applied to the flow over wall-mounted cubes. Int. J. Heat Fluid Flow **23**, 330–339 (2002). doi:10.1016/S0142-727X(02)00180-7
36. Schumann, U.: Subgrid scale model for finite difference simulations of turbulent flows in plane channels and annuli. J. Comput. Phys. **18**, 376–404 (1975). doi:10.1016/0021-9991(75)90093-5
37. Shih, T.-H., Liu, N.-S.: Modeling of internal reacting flows and external static stall flows using RANS and PRNS. Flow Turbul. Combust. **81**, 279–299 (2008). doi:10.1007/s10494-007-9097-z
38. Shih, T.-H., Liu, N.-S.: A nonlinear dynamic subscale model for PRNS/VLES of internal combustor flows. AIAA Paper 2009-467 (2009)
39. Smagorinsky, J.: General circulation experiments with the primitive equations. Mon. Weather Rev. **91**, 99–165 (1963). doi:10.1175/1520-0493(1963)091<0099:GCEWTP>2.3.CO;2
40. Spalart, P.R., Allmaras, S.R.: A one-equation turbulence model for aerodynamic flows. Rech. Aerospatiale **1**, 5–21 (1994)
41. Spalart, P.R., Jou, W.H., Strelets, M., Allmaras, S.R.: Comments on the Feasibility of LES for Wings and on a Hybrid RANS/LES Approach. Advances in DNS/LES. Greyden, New York (1997)
42. Speziale, C.G.: Turbulent modeling for time-dependent RANS and VLES: a review. AIAA J. **36**, 173–184 (1998). doi:10.2514/2.7499
43. Squires, K.D., Forsythe, J.R., Morton, S.A., Strang, W.Z., Wurtzler, K.E., Tomaro, R.F., Grismer, M.J., Spalart, P.R.: Progress on detached-eddy simulation of massively separated flows. AIAA Paper 2002-1021 (2002)
44. Strelets, M.: Detached-eddy simulation of massively separated flows. AIAA Paper 2001-0879 (2001)
45. Temmerman, L., Hadziabdic, M., Leschziner, M.A., Hanjalic, K.: A hybrid two-layer URANS-LES approach for large-eddy simulation at high Reynolds numbers. Int. J. Heat Fluid Flow **26**, 173–190 (2005). doi:10.1016/j.ijheatfluidflow.2004.07.006
46. Tucker, P.G., Davidson, L.: Zonal k–l based large-eddy simulations. Comput. Fluids **33**, 267–287 (2004). doi:10.1016/S0045-7930(03)00039-2
47. Versteeg, H.K., Malalasekera, W.: An Introduction to Computational Fluid Dynamics: The Finite Volume Method. Prentice Hall, Upper Saddle River (1995)